Green Chemistry

ROYAL SOCIETY OF CHEMISTRY

PAPER

View Article Online
View Journal | View Issue

Cite this: *Green Chem.*, 2025, **27**, 1519

Deep eutectic solvent-based microextraction system for simultaneous lignocellulose fractionation and furfural production†

Liu Liu, Qianwei Li and Caixia Wan *

A biomass conversion process with a microextraction system was developed for simultaneous lignocellulose fractionation and conversion. The liquid–liquid biphasic platform was composed of a deep eutectic solvent (DES) (polyethylene glycol : oxalic acid) and methyl isobutyl ketone (MIBK). Microemulsion (O/W) was formed on constant stirring and stabilized by sodium salt crystal, which also acted as an interphase catalyst to enhance furfural yields. Furfural was continuously extracted into MIBK after being formed in the DES. The highest furfural yield of 76.5% was obtained when the reaction was conducted at 150 °C for 60 min in the presence of 12.3 wt% NaCl. The extracted lignin was functionalized with polyethylene glycol, with substantial retention of the native structure of lignin. The pulp also showed high enzymatic digestibility of cellulose. This work demonstrated the role of salt crystals in stabilizing Pickering emulsions for microextraction and their function in simultaneous biomass fractionation and conversion for high-value platform chemicals, paving the way toward sustainable biorefineries.

Received 14th June 2024,
Accepted 25th November 2024

DOI: 10.1039/d4gc02874k

rsc.li/greenchem

1. Introduction

Furfural is one of the top value-added platform chemicals derived from biomass[1] and has a broad spectrum of industrial applications, such as in solvents, plastics, and pharmaceuticals.[2,3] Furfural is produced from pentose, with xylan-rich lignocellulosic biomass as an almost exclusive feedstock, as there is no synthetic route available for the conversion of petroleum to furfural.[3,4] Two main steps are involved in furfural production, *i.e.*, xylan hydrolysis into xylose, followed by xylose dehydration into furfural.[5] The prevailing furfural production method is primarily based on mineral acid-catalyzed reaction systems. However, such a process is energy intensive, generates large quantities of solid and liquid waste, and has low yields. With a growing market for furfural, it is important to address these drawbacks by developing more cost-effective strategies to promote the sustainable growth of the furfural industry.

Solvent systems based on green chemistry principles have been explored for furfural production. Deep eutectic solvents (DESs) composed of both hydrogen bond acceptor (HBA) and hydrogen bond donor (HBD) have been extensively explored for biomass pretreatment. DESs can function as both reaction media and catalysts, and most constituents are renewable, low-cost, and non-hazardous, providing an economic, environmentally friendly, and versatile alternative to traditional mineral acid-based catalysts. This makes DES a promising choice for the fractionation of lignocellulose and catalytic conversion of xylan into furfural. In particular, polyol-based DESs have been reported to be effective for dissolving lignin from biomass due to strong interactions between hydroxyl groups on polyols and those on lignin, leading to improved cellulase accessibility to cellulose pulp. Thus, such DESs represent a new class of designer solvents with unique surface tension and thermodynamic properties.[6]

Compared to DESs typically based on quaternary ammonium salts, the incorporation of polyols into DES formulations contributes to the enhanced stabilization of intermediates in biomass pretreatment. Liu *et al.*[7] developed a ternary DES by adding ethylene glycol (EG) to choline chloride (ChCl) : oxalic acid (OA). The presence of EG has been reported to stabilize carbocation and prevent the breakdown of β-O-4 linkages during pretreatment, leading to higher lignin extraction efficiency and greater selectivity of aromatic

Department of Chemical and Biomedical Engineering, University of Missouri, 1406 Rollins Street, Columbia, MO, 65211, USA. E-mail: wanca@missouri.edu; Tel: +1 573 884 7882

† Electronic supplementary information (ESI) available: Additional analysis and experimental section including quantitative analysis of 2D NMR spectrum of recovered lignin and enzymatic hydrolysis of pulp; detailed information of composition of biphasic solvent systems; additional results of thermal behavior, viscosity and acidity of DES; additional result of xylose conversion during fractionation; additional FTIR analysis of pulp; comparison of furfural production *via* different biphasic systems from biomass; additional experiment phenomenon of Pickering emulsion formation. See DOI: https://doi.org/10.1039/d4gc02874k

monomers *via* depolymerization. Xue *et al.*[8] designed ChCl : glycerol : polyethylene glycol (PEG) ternary DESs with excellent lignin dissolving ability. Polyols composed of glycerol/PEG were believed to participate in lignin liquefaction with intermolecular hydrogen bonding. Additionally, polyols were found to promote furfural conversion and slow down its degradation during prolonged reaction time.[9] Therefore, the rational design of polyol-based DESs capable of stabilizing xylose and other degradation intermediates will provide effective strategies for enhancing the efficiency of biomass fractionation and furfural production.

Furfural tends to degrade rapidly through resinization and self-condensation once synthesized, resulting in low yields. *In situ* extraction using a biphasic system is an effective way to minimize degradation and enhance furfural production. By introducing an organic phase into the solvent system, furfural can be continuously transferred to the organic phase, thereby reducing its concentration in the aqueous phase and minimizing degradation. Cheng *et al.*[10] developed a novel DES/γ-valerolactone (GVL) biphasic system based on DES (ChCl : OA, ChCl : *p*-toluenesulfonic acid) and GVL and achieved a 68.6% furfural yield. Nzediegwu *et al.*[11] developed a catalytic system comprising $AlCl_3$/LiCl/NaCl in H_2O/MIBK biphasic media, achieving production of furfural and hydroxymethylfurfural from corrugated boxes with maximum yields of 51% and 98% at 160 °C and 40 min, respectively. Castro *et al.*[12] reported furfural synthesis with a high yield of 77% in a biphasic system (butyl acetate and saturated NaCl solution) with the assistance of microwave at 160 °C for 10 min. Despite the advantages of biphasic systems, they have inherent mass transfer limitations associated with two phases.[13] This transfer barrier attributed to the limited interfacial contact can lead to rehydration and by product formation.[14] To address these challenges, a biphasic system based on Pickering emulsion looks promising for an effective fractionation process. The presence of the emulsion micelle was shown to significantly enhance mass transfer at the interface in a binary solvent system.[15]

In this study, DESs composed of PEG and oxalic acid (OA) were synthesized to enable biomass fractionation and simultaneous conversion of xylan to furfural. The addition of NaCl triggered the formation of a Pickering emulsion. Pretreatment effectiveness was evaluated by analyzing the chemical composition and enzymatic digestibility of the pulp. Lignin extracted *via* the biphasic reaction system was characterized for detailed chemistry. The effects of key reaction parameters, including NaCl/H_2O, reaction temperature, and time, on furfural yields and selectivity were also studied. The mechanism involved in lignocellulose fractionation and the catalytic synthesis of furfural at the interphase was also proposed.

2. Materials and methods

2.1 Materials

Switchgrass collected from South Farm at the University of Missouri was air-dried and ground through a 1-mm screen. It was mainly composed of 33.91 wt% cellulose, 23.45 wt% xylan, and 19.54 wt% lignin. Cellic® CTec2 and HTec2 were kindly provided by Novozyme (Franklinton, NC, USA). All the chemicals were of analytical grade and purchased from Fisher Scientific (Heysham, Lancashire, UK).

2.2 Biomass pretreatment

DESs were synthesized by mixing PEG400 and OA with the mole fraction of PEG (average M_n 400) ranging from 0 to 1 at 80 °C until forming a clear and transparent liquid. Biphasic solvent systems were prepared by mixing DES, MIBK, H_2O or NaCl solution (25 wt% NaCl content) with varied mass ratios specified in Table S1.† In a typical run of pretreatment, 2.0 g of air-dried switchgrass (9.5% moisture content) was mixed with 40.0 g of biphasic solvent in a 100 mL hydrothermal reactor. The reactor was heated to different temperatures (*i.e.*, 130, 140, 150, and 160 °C) for 60 min, or heated at 150 °C for varying durations (*i.e.*, 20, 40, 60, 80, and 100 min) with constant magnetic stirring at 800 rpm. Thereafter, the reactor was cooled to room temperature, followed by the addition of 100 mL of water. The solid residues and liquids were collected separately by vacuum filtration. The filtrate (*i.e.*, liquid fraction) was further separated into aqueous and organic phases in a separatory funnel, and each phase was subjected to furfural analysis. Lignin was recovered by washing the solid residues with aqueous acetone (60%, w/w), followed by acetone removal and then freeze-dried. The pulp resulting from lignin removal was subjected to enzymatic hydrolysis as detailed in the ESI.†

2.3 Characterization

The concentrations of furfural, xylose, and glucose were determined using HPLC (Agilent 1100 series) equipped with a diode array detector (DAD, 268 nm) and a refractive index detector (RID). An Aminex HPX-87H column was used for the analysis of furfural in the aqueous phase and monomeric sugars (*i.e.*, glucose and xylose), and the mobile phase was 5 mM sulfuric acid, eluting at 0.6 mL min^{-1}. The temperatures of the column and RID were maintained at 65 °C and 40 °C, respectively. The Phenomenex Luna C18(2) column was used to analyze furfural in the organic phase, and the mobile phase was methanol/water (20/80, v/v), eluting at 0.8 mL min^{-1} at 30 °C. All the samples were filtered through a 0.22 μm nylon syringe filter prior to HPLC analysis.

Furfural yield, xylose conversion, and furfural selectivity were calculated using eqn 1, 2 and 3. Lignin and cellulose contents in switchgrass were determined following the NREL Laboratory Analytical Procedure, as detailed in the ESI.†[16]

$$\text{Furfural yield}\,(\%) = \frac{\text{moles of furfural produced}}{\text{moles of xylose in raw switchgrass}} \times 100\%\,, \quad (1)$$

$$\text{Xylose conversion}\,(\%) = \frac{\text{moles of xylose converted}}{\text{moles of xylose in raw switchgrass}} \times 100\%, \quad (2)$$

$$\text{Furfural selectivity}\,(\%) = \frac{\text{moles of furfural produced}}{\text{moles of xylose converted}} \times 100\%, \quad (3)$$

FTIR spectra were acquired on a Nicolet 4700 FTIR spectrometer attached with ATR. The samples were scanned from the 500 to 4000 cm^{-1} range at room temperature with a resolution of 4 cm^{-1} and an accumulation of 64 scans. ^{1}H–^{13}C HSQC spectrum was acquired using a Bruker Avance III 600 MHz NMR spectrometer. The analysis was carried out at 323 K with acquisition parameters as follows: the "Hsqcedetgp" pulse program with spectral widths of 9014 Hz (from 15 to 0 ppm) and 25 635 Hz (from 170 to 0 ppm) for the ^{1}H- and ^{13}C-dimensions; the size of FID was set as 1024 (F2) and 256 (F1) with the number of scans of 32. The NMR spectrum was processed using MestReNova version 15.0.0.

Rheological properties were analysed using an Anton Parr SmartPave 102 rotational rheometer equipped with 25 mm plate geometry. Static viscosity was measured at a sheer rate of 10 s^{-1}. Dynamic properties were determined in the frequency sweep mode with angular frequency ranging from 0.1 to 100 rad s^{-1}.

Thermal properties were analyzed using TA Instruments DSC Q20 Differential Scanning Calorimeter. Melting points were determined under a 20 mL min^{-1} nitrogen flow. Samples (6–8 mg) were sealed in aluminum pans, and the temperature was ramped to 80 °C at a heating rate of 10 °C min^{-1} and equilibrated at that temperature for 5 min. Afterwards, the samples were cooled to −70 °C at a cooling rate of 5 °C min^{-1}, held at the same temperature for 5 min, and finally reheated to 80 °C at a heating rate of 5 °C min^{-1}. The melting enthalpy was integrated from the endothermic peak area from the second heating cycle using TA Universal Analysis software.

3. Results and discussion

3.1 Hydrogen bond formation in DES

The hydrogen bonding interactions in DES are the main driving force for biomass fractionation.[17] These interactions indicate the reactivity of the biomass pretreatment system. The hydrogen bond network in DES was characterized by thermal properties, rheological properties, and functional groups. The melting point of pure PEG 400 is −10.37 °C (Fig. 1a), while that of OA is 98 °C. By varying the molar fraction of PEG (χ_{PEG}), the DESs exhibited a phase transition from solid to liquid at room temperature (Fig. 1b), along with corresponding changes in melting points. The melting points of the PEG : OA mixtures were lower than those of the individual components. The eutectic point of DES with χ_{PEG} of 0.5 had a minimum melting point of −63.94 °C, which was much lower than that of DESs reported previously.[18] This decrease in melting point was associated with the formation of hydrogen bonding between PEG and OA, which reduced the lattice energy of the eutectic solvent.[19] The lowest melting enthalpy (5.05 J g^{-1}) was also observed at the eutectic point (Table S2†), indicating a shorter range and weaker configuration of hydrogen bonds compared to non-eutectic points on the phase diagram. This finding agreed with previously reported trends in surface tension.[20] Such a unique structural feature allowed DES to easily disrupt internal hydrogen bonds and form competitive hydrogen bonds with substances, thereby improving their dissolving capabilities.[21] Considering the strong potential for biomass fractionation, DES (χ_{PEG} = 0.5) was thus used for the proposed biomass pretreatment.

The viscoelasticity of DES differed notably from that of pure PEG, demonstrating alterations in the solvent structure (Fig. 1c and d). For PEG (Fig. 1c), the initial loss modulus (G'') was higher than the storage modulus (G'). Although both G' and G'' increased with angular frequency, G'' remained consistently higher. The dominance of G'' indicated that PEG 400 exhibited more viscous behavior than the elastic one under applied deformation or stress. In contrast, PEG : OA initially showed that G' was higher than G'' (Fig. 1d). The crossover of G' and G'' at increasing frequencies suggested that the DES behaved like a weak gel with entangled polymer chains, indicating a topological network.[22] This behavior validated the presence of strong hydrogen bonding, which remained highly crosslinked at low shear force but became vulnerable at high shear force. At lower frequencies (<4 rad s^{-1}), DES exhibited more crosslinked structures, leading to the dominance of elastic behavior ($G' > G''$). However, at higher frequencies (>4 rad s^{-1}), part of the hydrogen bonds in the DES was disrupted, resulting in dominant viscous behavior ($G'' > G'$).

The formation of hydrogen bonds between PEG and OA was further investigated using FTIR to gain deeper structural insights. As depicted in Fig. 1e, the FITR spectrum of PEG showed peaks at 3447 cm^{-1} for O–H stretching (hydroxyl), 2869 cm^{-1} for the C–H stretching of methylene, and 1103 cm^{-1} for C–O stretching (ether). After PEG was combined with OA to form DES (χ_{PEG} = 0.5), the O–H stretching vibration peak around 3447 cm^{-1} became broader, indicating the formation of hydrogen bonds. The blue-shifting of C–H to 2876 cm^{-1} was inferably caused by the strong repulsion when approaching OA, inducing electron density redistribution within the pair of C–H (from PEG)···O (from OA) hydrogen bonding.[23,24] The formation of hydrogen bonds also accounted for the red-shifting of the C–O stretching absorption peak to 1099 cm^{-1}, possibly originating from the attraction between protons (H–OOC– from OA) and HBA (the C–O from PEG).[25]

Adding water is necessary to address the mass transfer limitation caused by the high viscosity of DES (215.17 mPa s, 3.4 times that of pure PEG, Table S3†) in biomass fractionation.[26] However, the hydrogen bond formation in DES was sensitive to water content, as indicated by the high correlation between solvent viscosity and intermolecular interaction. To

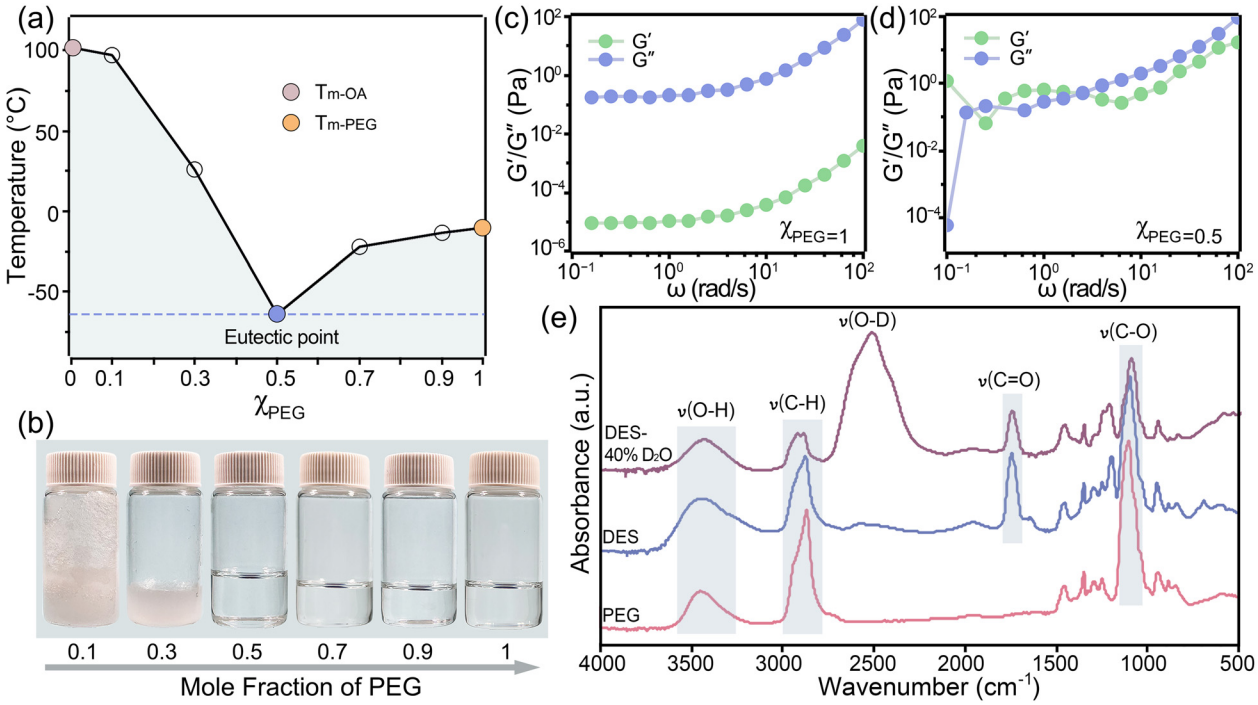

Fig. 1 DES property and structure. (a) Phase diagram of PEG : OA binary DES. $T_{m\text{-}OA}$ and $T_{m\text{-}PEG}$ are the melting points of OA and PEG, respectively; the blue dashed line is the eutectic temperature; χ_{PEG} is the mole fraction of PEG in DES. (b) Photographs of DES samples with varied χ_{PEG}. (c) and (d) Viscoelastic behaviors of pure PEG (χ_{PEG} = 1) and DES (χ_{PEG} = 0.5), respectively. (e) FTIR spectra of PEG, DES (χ_{PEG} = 0.5), and DES (χ_{PEG} = 0.5) containing 40% D_2O.

evaluate the hydration effect on the hydrogen-bond-driven network structure of DES, 40% deuterated water (D_2O) was added. As shown in Fig. 1e, after adding D_2O, the O–H band was red-shifted from 3446 to 3435 cm^{-1}, and the C–O band was red-shifted from 1099 to 1093 cm^{-1}. The peak at 1745 cm^{-1} was assigned to the C=O stretching of the carboxyl group. A strong peak centered at 2500 cm^{-1} was assigned to the O–D stretching band, and the peak at 1214 cm^{-1} was assigned to the δ(D–O–D) bending band. The redshift of O–D and blueshift of C–H stretching bands were detected with increasing D_2O content (data not shown). The observed redshift of O–D might be attributed to the partial self-aggregation of water molecules. It can also be inferred that water content affects intermolecular interactions by forming multiple hydrogen bonds with PEG and OA.

3.2 Microemulsion formation of DES-based biphasic system

Xylose-to-furfural conversion is typically conducted at high temperatures and/or for a long reaction time.[27] Under a typical reaction condition (150 °C, 60 min), degradation of certain DES components was observed, accompanied by the generation of formic acid, as detected *via* HPLC (Fig. S1†). As illustrated in Fig. 2a, adding NaCl solution to DES ($D_{42}S_{28}$) significantly alleviated the degradation of OA, decreasing its mass reduction from 50.0% to 21.5%. PEG was more stable in this system, showing minor loss (3.5%–7.7%). The partition of furfural in this biphasic system was investigated at a MIBK/DES (with water) ratio of 30 : 70, as shown in Fig. 2b. Furfural solubility in the MIBK phase increased with the increase of water content in DES. Moreover, the addition of water and NaCl, particularly NaCl, increased the partition coefficient of furfural in the organic phase (Fig. 2b).

Interestingly, the NaCl-containing biphasic system became emulsified upon vigorous agitation (Fig. S2b†) regardless of temperature, and the emulsion remained stable with continuous agitation (Fig. 2c–e). PEG, being amphiphilic, is commonly used as an emulsifier to prepare O/W emulsions.[28] Its emulsifiability was enhanced in the presence of NaCl. Salt microcrystals were formed surrounding the micelles in emulsions (Fig. 2d and e), increasing the contact areas between substrates and salt crystals. PEG introduced depletion interactions into the interphase of emulsion droplets and sodium microcrystals. This attractive interaction facilitated the adsorption of sodium microcrystals onto the droplet surface and simultaneously suppressed desorption once adsorbed, inhibiting phase inversion and providing great stability.[29] Stabilized emulsion micelles could protect furfural from side reactions in the acidic DES phase. Such emulsion systems acted as microcarriers to confine MIBK in the aqueous phase, increasing the interfacial area and improving furfural extraction. The biphasic system was demulsified when sodium crystals settled without stirring. The saturated NaCl facilitated the phase separation of DES and MIBK (Fig. 2c), promoting the furfural partition into the organic phase.

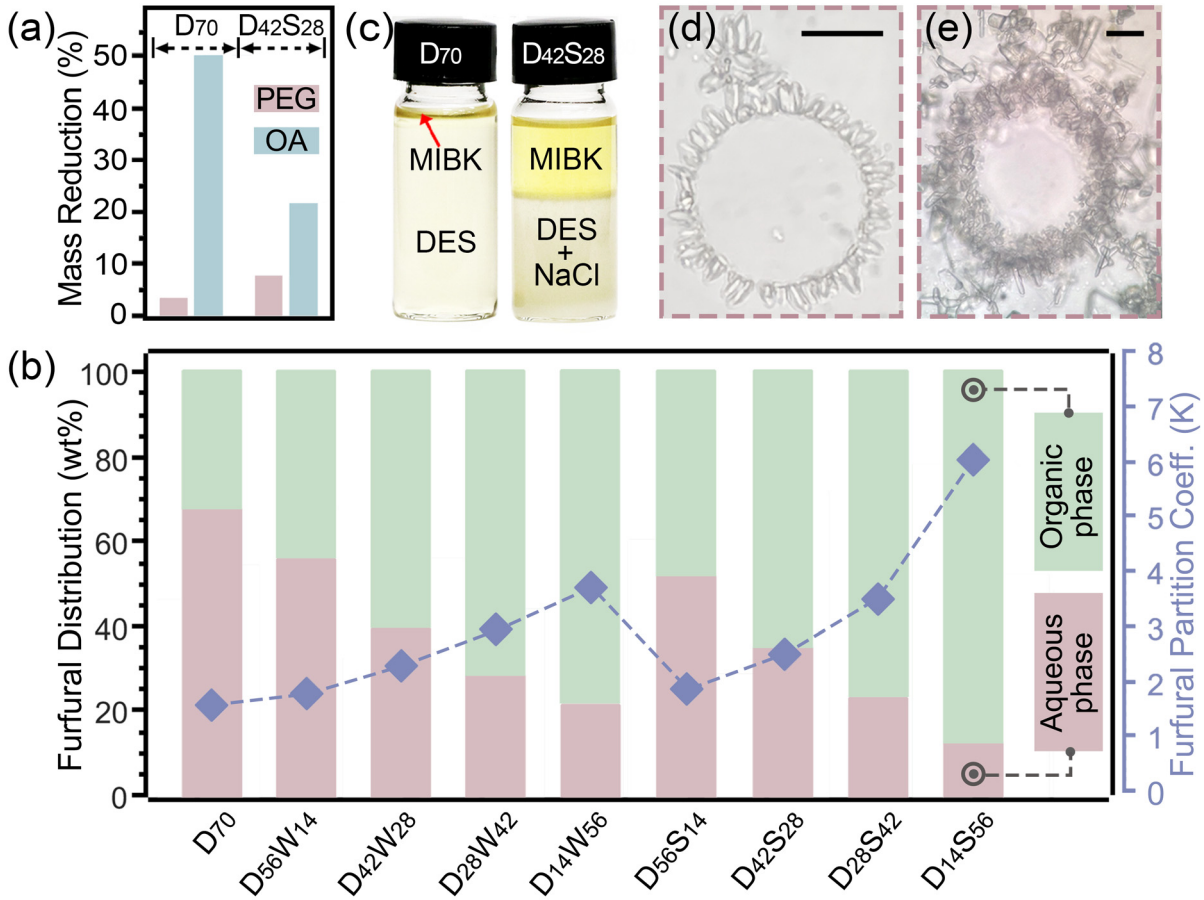

Fig. 2 Effect of NaCl on DES-MIBK biphasic solvent. (a) Thermal stability (mass reduction percentage) of DES constituents after heating at 150 °C for 60 min. (b) Furfural distribution percentage (stacked bar chart) and partition coefficients (*K*, line chart) in the biphasic system at room temperature (25 ± 1 °C). (c) Photos of cooled biphasic solvent after heating at 150 °C for 60 min. Micrographs of micelle in emulsion at (d) room temperature (25 ± 1 °C) and (e) after heating at 150 °C for 60 min (scale bars: 15 μm).

3.3 Pretreatment effectiveness

The compositions and enzymatic digestibility of the pulp recovered from the biphasic reaction system were analyzed to evaluate the fractionation effectiveness. In particular, the effects of NaCl content in reaction media were investigated under a representative reaction condition (150 °C for 60 min). The resulting pulp contained 71%–79% glucan and 14%–23% lignin but no xylan (Fig. 3a). The lignin content in the pulp reached the highest (23%) when the NaCl solution was 28% ($D_{42}S_{28}$, corresponding to 7% NaCl). The enzymatic digestibility of cellulose in the pulp ranged from 74.6% to 88.0% (Fig. 3b). In general, pulp with lower lignin content tends to be more digestible due to the high accessibility to cellulase enzymes.[30] Surprisingly, the pulp containing the highest lignin content (23%) resulting from $D_{42}S_{28}$ treatment showed the highest enzymatic digestibility (88%) under the sub-optimal enzymatic hydrolysis condition. This could be attributed to the lignin modification by PEG during the fractionation, which subsequently reduced the non-productive cellulase adsorption.[31] The FTIR spectrum of pulp from $D_{42}S_{28}$ (Fig. S3, with band assignments in Table S8†) displayed C–O stretching vibration, possibly originating from PEG and/or OA, at 1104 cm^{-1}, which suggests the modification of pulp and lignin by those DES constituents. The out-of-plane bending vibrations of crystalline cellulose appeared at 777 and 721 cm^{-1}. In raw switchgrass, an out-of-plane bending vibration of C–H in lignin was observed at 986 cm^{-1}, but this band disappeared in the pulp. These results indicated that the majority of lignin was removed during treatment, leaving cellulose exposed.

Increasing NaCl from 7% to 12.3–14% caused a decline in digestibility, even with a lower lignin content. For example, the pulp resulting from $D_{56}S_{14}$ and $D_{14}S_{56}$ pretreatment, containing similar lignin and cellulose contents, showed different enzymatic digestibility (87.5% and 74.6%, respectively). High NaCl content in the $D_{14}S_{56}$ pretreatment promoted undesired reactions, resulting in the formation of pseudolignin and condensed lignin,[32] which in turn could deposit onto the surface of the cellulose, lowering the enzymatic hydrolysis efficiency. Moreover, the reduced PEG content in the $D_{14}S_{56}$ treatment significantly decreased the lignin–PEG interactions. In short,

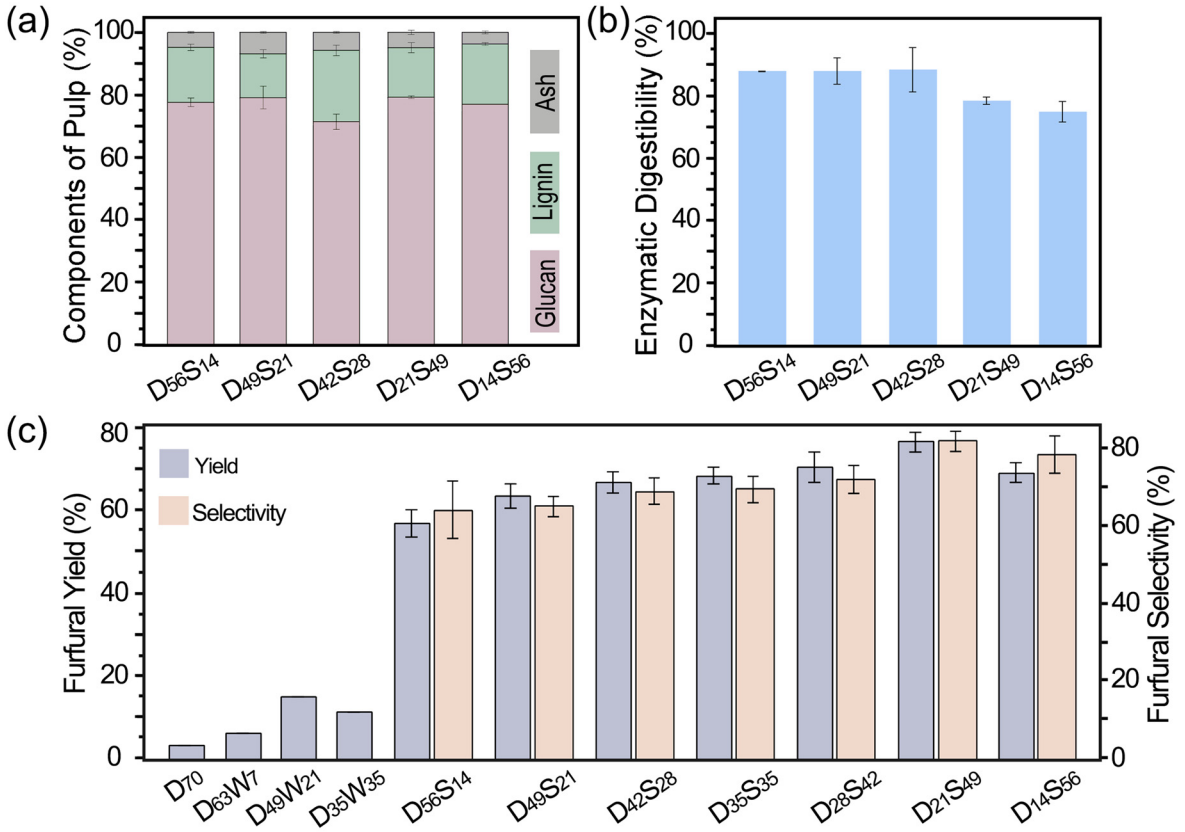

Fig. 3 Effect of NaCl content on the pulp quality and furfural production. (a) Component percentage of pulp, (b) enzymatic digestibility of pulp, and (c) furfural yield and selectivity.

this pretreatment system can separate cellulose and lignin with high efficiency, and it can also be inferred that high NaCl content induces negative modifications of pulp chemistry, directly influencing enzymatic hydrolysis, although delignification efficiency may not change noticeably.

3.4 Furfural production

Furfural formation simultaneously occurred during the pretreatment, which was further investigated under the reaction condition of 150 °C for 60 min. The study on the water effect showed that furfural yield was improved when using hydrated DES ($D_{63}W_7$, $D_{49}W_{21}$, and $D_{35}W_{35}$) for fractionation compared to using pure DES (D_{70}) in the biphasic system (Fig. 3c). The DES/MIBK system containing 21% water reached the highest furfural yield of 14.62%, while the biphasic system with 7% water content had the lowest yield. Compared to furfural production using pure DES, the use of hydrated DES resulted in an almost up to 4-fold increase in yield. However, the furfural yields obtained under these conditions were still unsatisfying.

Impressively, replacing water with the same quantity of NaCl solution increased furfural yield more than 5 times under the same condition ($D_{49}W_{21}$ *vs.* $D_{49}S_{21}$). NaCl should play a dual role in furfural production with an improved yield. One role was to catalyze the xylose-to-furfural conversion as a metal chloride salt, similar to that reported in prior studies.[33] The other role was to facilitate the formation of a microemulsion, which enhanced the extraction of furfural into the organic phase. The furfural yield increased with the increase in NaCl content and reached the highest yield of 76.5% in the presence of 12.3% NaCl. The furfural selectivity showed a similar trend, with the highest being 82.02% (Fig. 3c). Both furfural yield and selectivity decreased with a further increase in NaCl content. Excess NaCl reduces the acidity of the reaction medium, resulting in insufficient xylose conversion accompanied by an increased side reaction associated with furfural degradation into humin. The high water content in the biphasic system could also reduce its reactivity. Consequently, xylose conversion decreased from 94.19% in $D_{28}S_{49}$ to 88.01% in $D_{14}S_{56}$ (Table S4†), and furfural selectivity did not increase.

The effects of reaction time and temperature on furfural production were also studied (Fig. 4). The complete xylose conversion along with the highest furfural yield was obtained when the reaction time for $D_{42}S_{28}$ was 80 min at 150 °C (Fig. 4a). Prolonging the reaction time at the same temperature led to reduced furfural yield due to side reactions under server conditions, while shortening the reaction time to 60 min would be beneficial for furfural selectivity. The darkening color of the solid residue also suggested a severe reaction with a prolonged time (Fig. 4b). For the pretreatment using the same DES, increasing the temperature from 130 to 160 °C at a

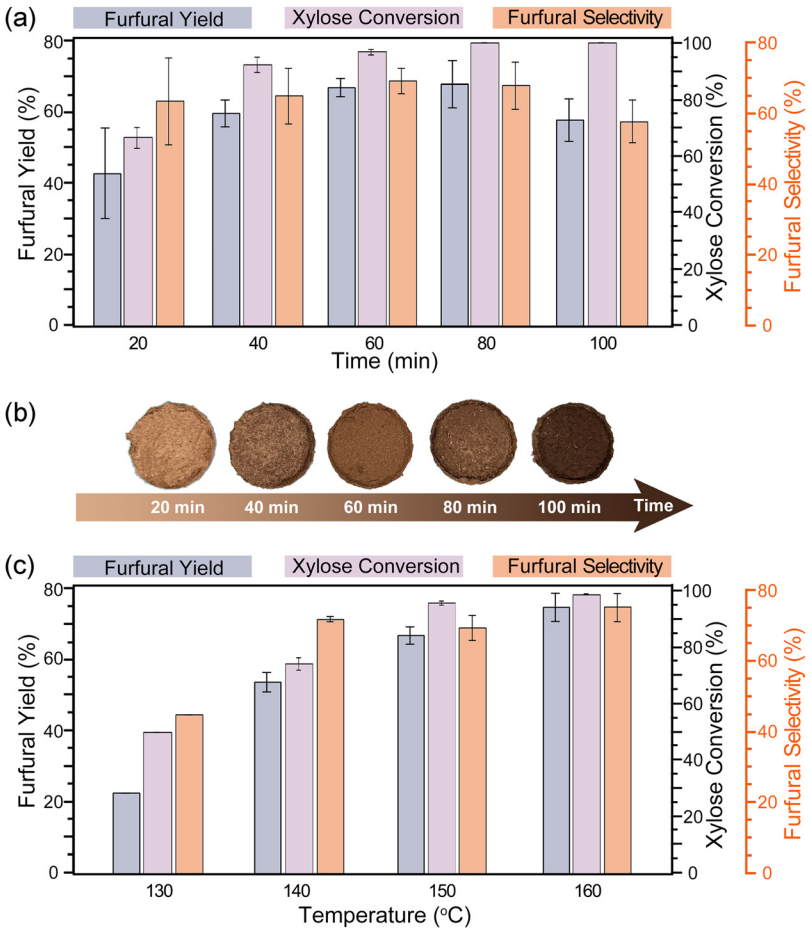

Fig. 4 Effect of reaction time and temperature. (a) Furfural yield, furfural selectivity and xylose conversion at 150 °C at varied times; (b) photographs of solid residues obtained at 150 °C at varied times; and (c) furfural yield, furfural selectivity and xylose conversion at 60 min with varied temperatures.

given time (60 min) favored the xylose dehydration into furfural with the higher yield, reaching the highest yield of 74.8% and selectivity of 74.9% at 160 °C (Fig. 4c). Although $D_{42}S_{28}$ required a longer time or higher temperature to maximize furfural yields, it appeared to be less effective than $D_{49}S_{21}$ discussed above. These findings suggest that an optimal condition for lignocellulose/xylan-to-furfural in a single step can be DES-specific. However, properly increasing NaCl and water content in the reaction media can boost furfural production under less severe reaction conditions.

3.5 Lignin chemistry

The 2D HSQC NMR spectrum of PEG-*g*-lignin extracted from the biphasic reaction system ($D_{42}S_{28}$, 150 °C, 60 min) revealed signals of the main lignin inter-monomeric units and the polymer chain end-units (Fig. 5a and b, respectively), showing similar side chains and aromatic regions to the cellulolytic enzyme lignin (CEL) of our previous study.[34] As depicted in Fig. 5a, β-aryl ether unit (β-O-4, Aα), phenyl coumarin unit (β-5, Bα), and resinol unit (β–β, Cα) interlinkages were detected at $\delta C/\delta H$ 71.32/4.89, 86.60/5.49, and 84.61/4.64 ppm, respectively. The β-position of β–β (C_β) signals was centered at 53.05/3.11 ppm. γ-Position of β-5 (B_γ) and β–β (C_γ) were at 62.02/3.70, and 70.66/4.17 ppm, respectively. Compared to CEL, new signals assigned to α-PEG-β-O-4 units (A′) and substituted PEG chains (P) were recognized at 80.62/4.67 (A′α), 59.70/3.48 (P_1), 69.33/3.5 ($P_{3/4}$), and 71.99/3.42 (P_2). A′$_\gamma$ of γ-acetylated β-O-4 linkage was detected at 59.70/3.64 ppm.[35] Volume integration analysis revealed that the β-O-4 interlinkage in the PEG-*g*-lignin accounted for 18.25%, β-5 for 0.37%, and β–β linkages for 2.44% (Table S5†). The partial retention of β-O-4 in PEG-*g*-lignin compared with CEL (46.7%) suggested the dissociation of this interlinkage during the fractionation. According to the NMR spectrum, PEGylation occurred on the α-position of β-O-4 structure (A′ in Fig. 5) and converted α-OH-β-O-4 to α-PEG-β-O-4 linkage.[36] Thus, PEG was grafted onto the α-position of the β-O-4 structure of lignin during the fractionation.

The main cross-signals in the aromatic region of PEG-*g*-lignin correspond to syringyl (S), guaiacyl (G), and *p*-hydroxyphenyl (H) units. Compared with CEL,[34] PEG-*g*-lignin showed a shrinkage of contours for S and G units, and the S/G ratio of PEG-*g*-lignin (S/G = 1.47) was higher than that of CEL (S/G = 0.7).

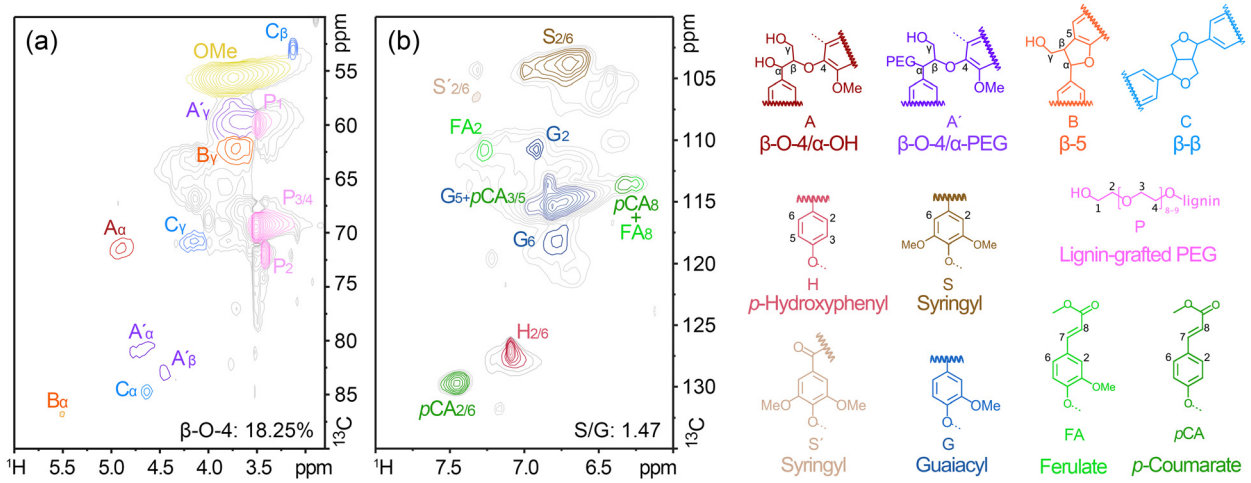

Fig. 5 2D HSQC NMR spectra of PEG-*g*-lignin obtained from the biphasic fractionation process. (a) Side-chain region (δC/δH 90–50/6.0–2.75) and (b) aromatic region (δC/δH 135–100/8.0–6.0).

Plausibly, the reduced intensity of S and G was due to the condensed structure formed during the fractionation process. Condensation at 2-, 5-, and 6-positions makes it lack hydrogen signals in HSQC NMR.[34,37] The increased S/G ratio suggests that lignin fragments rich in G-units tend to condense. Prominent signals corresponding to ferulate (FA) and *p*-coumarate (*p*CA) were also detected in the aromatic region of PEG-*g*-lignin.[38] The cross-peak centered at δC/δH 129.84/7.45 ppm was attributed to $pCA_{2/6}$, and the correlation peak of $pCA_{3/5}$ overlapped with G5 around 114.91/6.72 ppm. The signal for FA_2 was observed to be around 110.91/7.27 ppm. The cross-peaks for vinyl carbons in *p*CA and FA structures overlapped around C_8/H_8 113.56/6.25–6.32 ppm.

3.6 Proposed reaction mechanism

PEG-based DES successfully broke down most interlinkages in the lignocellulose complex in switchgrass. The possible mechanism for xylan to furfural is illustrated in Fig. 6. OA acted as the primary acid catalyst, depolymerizing xylan by protonating the hydroxyl groups and facilitating the cleavage of glycosidic bonds. The depolymerization released xylose, which was subsequently isomerized into 1,2-enediol under acidic conditions. NaCl, with its strong hydration effect compared to hydrogen ions (H^+), enhanced the acidity of the reaction medium by releasing and increasing the activity of free H^+.[39] The addition of NaCl significantly decreased the pH, resulting

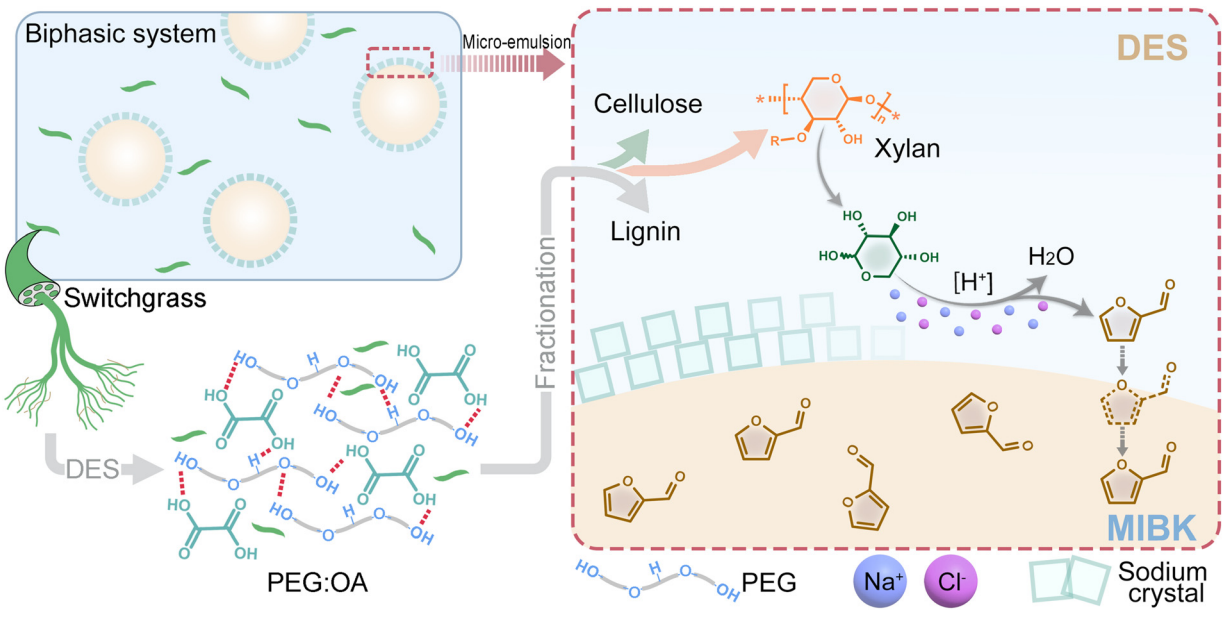

Fig. 6 Schematic of lignocellulose fractionation and interfacial catalysis for furfural formation.

in the DES/NaCl mixture with a lower value of pH than either pure DES or NaCl solution (Table S6†). The increased acidity further promoted the depolymerization of xylan and the isomerization of xylose. The presence of Cl^-, functioning as an electron donor in Lewis acid, facilitated the formation of 1,2-enediol. The subsequent H^+-catalyzed dehydration of 1,2-enediol led to cyclization and the formation of furfural.[40]

The furfural yield obtained under the optimized DES condition ($D_{21}S_{49}$, 150 °C, 60 min) in this study was higher than those obtained from most reactions previously reported using lignocellulose as a substrate and even comparable to those using pure xylose (Table S7†).[41,42] A possible reason for this high furfural yield was the rapid reaction rate facilitated by Cl^- from metal chloride salt, which outpaced side reactions, resulting in enhanced furfural production. Another contributing factor could be the stabilization of emulsion micelles by recrystallized salts, primarily sodium chloride crystals, with the possible inclusion of sodium oxalate. Salt crystals appeared immediately by mixing PEG-based DES with NaCl solution. With mixing, solvent diffusion occurred at the liquid–liquid interface, potentially forming PEG-H_2O supramolecular complexes, causing supersaturation at the interfacial area and enabling crystal formation.[28,43] In the meantime, oil-in-water (O/W) droplets were generated, and sodium salt crystals provided nucleation sites to promote micelles formation.

Additionally, sodium salts were proven to reduce the electrostatic repulsion among the surfactant head groups, facilitating the self-aggregation of PEG and reducing the critical micelle concentration in the emulsion.[44] Crystals were simultaneously adsorbed to the O/W micelle interface, helping to stabilize the O/W structure, which is the typical function of particles in Pickering emulsions.[45] The accumulation of salt crystals around the emulsion micelles resulted in concentrated free ions, including H^+, at the micellar interface. Given the noticeable catalytic effects of metal chloride salts, the main catalytic reactions likely occurred at the micelle interface. In the meantime, furfural was transferred to the organic phase of O/W micelle, driven by the PEG chains and salting-out effect of sodium salt, achieving efficient extraction while minimizing side reactions.

4. Conclusions

The polyethylene glycol (PEG) : oxalic acid (OA) deep eutectic solvent (DES)-based biphasic system demonstrates significant promise as a novel reaction system for biomass conversion. Enhanced hydrogen bonding interactions improved the dissolution and pretreatment efficiency of DES, promoting the effective fractionation of switchgrass. Xylan was selectively converted to furfural with NaCl as a catalyst, which reduced OA degradation, enhanced PEG stability, and improved furfural partition into the organic phase. The sodium salt crystals triggered the formation of O/W microemulsion, facilitating the continuous furfural conversion and extraction. A maximum furfural yield of 76.5% was achieved in the presence of 12.3% NaCl in the DES under reaction conditions of 150 °C and 60 min. The cellulose pulp had the highest enzymatic digestibility of 88% while containing 14–23% lignin. The extracted lignin showed PEG-functionalized motifs and partially preserved β-O-4 interlinkage. The proposed biphasic solvent system provides an efficient approach for biomass fractionation and the simultaneous conversion of xylan to furfural *via* process intensification to maximize biomass conversion.

Data availability

The authors confirm that the data supporting the findings of this study are available within the article and its ESI.†

Conflicts of interest

There is no conflict of interest to declare.

Acknowledgements

This work was financially supported by the USDA National Institute of Food and Agriculture (award no. 2021-67021-34504).

References

1 J. J. Bozell and G. R. Petersen, *Green Chem.*, 2010, **12**, 539–554.
2 C. M. Cai, T. Zhang, R. Kumar and C. E. Wyman, *J. Chem. Technol. Biotechnol.*, 2014, **89**, 2–10.
3 L. Zhang, H. Yu, P. Wang, H. Dong and X. Peng, *Bioresour. Technol.*, 2013, **130**, 110–116.
4 S. Peleteiro, S. Rivas, J. L. Alonso, V. Santos and J. C. Parajó, *Bioresour. Technol.*, 2016, **202**, 181–191.
5 A. S. Mamman, J. M. Lee, Y. C. Kim, I. T. Hwang, N. J. Park, Y. K. Hwang, J. S. Chang and J. S. Hwang, *Biofuels, Bioprod. Biorefin.*, 2008, **2**, 438–454.
6 Y. Chen, L. Fu, Z. Liu, F. Dai, Z. Dong, D. Li, H. Liu, D. Zhao and Y. Lou, *J. Mol. Liq.*, 2020, **318**, 114042.
7 Y. Liu, N. Deak, Z. Wang, H. Yu, L. Hameleers, E. Jurak, P. J. Deuss and K. Barta, *Nat. Commun.*, 2021, **12**, 5424.
8 B. Xue, Y. Yang, R. Tang, D. Xue, Y. Sun and X. Li, *Int. J. Biol. Macromol.*, 2020, **164**, 480–488.
9 D. Xu, W. Tang, Z. Tang and Y. He, *Catalysts*, 2023, **13**, 467.
10 J. Cheng, C. Huang, Y. Zhan, X. Liu, J. Wang, C. Huang, G. Fang, A. J. Ragauskas, Z. Xie and X. Meng, *Bioresour. Technol.*, 2023, **387**, 129653.
11 E. Nzediegwu and M.-J. Dumont, *Cellulose*, 2023, **30**, 4957–4970.
12 G. A. D. Castro, R. C. Batista, R. d. C. S. de Sousa, A. d. C. O. Carneiro and S. A. Fernandes, *React. Chem. Eng.*, 2023, **8**, 1969–1980.
13 M. Pera-Titus, L. Leclercq, J. M. Clacens, F. De Campo and V. Nardello-Rataj, *Angew. Chem., Int. Ed.*, 2015, **54**, 2006–2021.

14 Z.-Q. Liu, J.-L. Guo, R.-H. Liang, F.-X. Wang, Z.-K. Li, Y. Liu and A. Ying, *Chem. Eng. J.*, 2024, **479**, 147757.
15 M. Jiang, J. Tan, Y. Chen, W. Zhang, P. Chen, Y. Tang and Q. Gao, *Chem. Commun.*, 2023, **59**, 3103–3106.
16 A. Sluiter, B. Hames, R. Ruiz, C. Scarlata, J. Sluiter, D. Templeton and D. Crocker, *Laboratory analytical procedure*, 2008, **1617**, 1–16.
17 X.-D. Hou, A.-L. Li, K.-P. Lin, Y.-Y. Wang, Z.-Y. Kuang and S.-L. Cao, *Bioresour. Technol.*, 2018, **249**, 261–267.
18 E. L. Smith, A. P. Abbott and K. S. Ryder, *Chem. Rev.*, 2014, **114**, 11060–11082.
19 Z. Li and P. I. Lee, *Int. J. Pharm.*, 2016, **505**, 283–288.
20 M. Fronduti, T. Del Giacco, E. Rossi, M. Tiecco and R. Germani, *J. Mol. Liq.*, 2023, **379**, 121679.
21 Q. Xia, Y. Liu, J. Meng, W. Cheng, W. Chen, S. Liu, Y. Liu, J. Li and H. Yu, *Green Chem.*, 2018, **20**, 2711–2721.
22 A. K. Das, M. Sharma, D. Mondal and K. Prasad, *Carbohydr. Polym.*, 2016, **136**, 930–935.
23 X. Chang, Y. Zhang, X. Weng, P. Su, W. Wu and Y. Mo, *J. Phys. Chem. A*, 2016, **120**, 2749–2756.
24 Y. Yang, W. Zhang and X. Gao, *Int. J. Quantum Chem.*, 2006, **106**, 1199–1207.
25 Y. Gu, T. Kar and S. Scheiner, *J. Am. Chem. Soc.*, 1999, **121**, 9411–9422.
26 K. D. O. Vigier, G. Chatel and F. Jérôme, *ChemCatChem*, 2015, **7**, 1250–1260.
27 A. Jaswal, P. P. Singh and T. Mondal, *Green Chem.*, 2022, **24**, 510–551.
28 Z. Wang, J. Song, S. Zhang, X.-Q. Xu and Y. Wang, *Langmuir*, 2017, **33**, 9160–9169.
29 K. Kim, S. Kim, J. Ryu, J. Jeon, S. G. Jang, H. Kim, D.-G. Gweon, W. B. Im, Y. Han and H. Kim, *Nat. Commun.*, 2017, **8**, 14305.
30 M. Takada, R. Chandra, J. Wu and J. N. Saddler, *Bioresour. Technol.*, 2020, **302**, 122895.
31 C. Lai, Y. Jia, C. Yang, L. Chen, H. Shi and Q. Yong, *ACS Sustainable Chem. Eng.*, 2020, **8**, 1797–1804.
32 C. Huang, W. Lin, Y. Zheng, X. Zhao, A. Ragauskas and X. Meng, *Green Chem.*, 2022, **24**, 5263–5279.
33 N. Zhou, C. Zhang, Y. Cao, J. Zhan, J. Fan, J. H. Clark and S. Zhang, *J. Cleaner Prod.*, 2021, **311**, 127780.
34 Z. Chen, X. Bai, L. A. , H. Zhang and C. Wan, *ACS Sustainable Chem. Eng.*, 2020, **8**, 9783–9793.
35 J. Cheng, X. Liu, Y. Zhan, J. Wang, X. Meng, X. Zhou, C. G. Yoo, C. Huang, C. Huang and G. Fang, *ChemSusChem*, 2023, e202301161.
36 T. T. Nge, Y. Tobimatsu, S. Takahashi, E. Takata, M. Yamamura, Y. Miyagawa, T. Ikeda, T. Umezawa and T. Yamada, *ACS Sustainable Chem. Eng.*, 2018, **6**, 7841–7848.
37 J.-L. Wen, T.-Q. Yuan, S.-L. Sun, F. Xu and R.-C. Sun, *Green Chem.*, 2014, **16**, 181–190.
38 J. C. del Río, J. Rencoret, G. Marques, A. Gutiérrez, D. Ibarra, J. I. Santos, J. Jiménez-Barbero, L. Zhang and Á. T. Martínez, *J. Agric. Food Chem.*, 2008, **56**, 9525–9534.
39 F. E. Critchfield and J. B. Johnson, *Anal. Chem.*, 1959, **31**, 570–572.
40 J. N. M. Soetedjo, C. B. Rasrendra and H. J. Heeres, *IOP Conference Series: Materials Science and Engineering*, 2020, **742**, 012049.
41 D. M. E. Delgadillo, G. A. D. Castro and S. A. Fernandes, *React. Chem. Eng.*, 2024, **9**, 1560–1568.
42 S. Wang, Y. Zhao, H. Lin, J. Chen, L. Zhu and Z. Luo, *Green Chem.*, 2017, **19**, 3869–3879.
43 W. Zhang, Y. Zhu, X. Liu, D. Wang, J. Li, L. Jiang and J. Jin, *Angew. Chem., Int. Ed.*, 2014, **53**, 856–860.
44 S. Aktar, M. Saha, S. Mahbub, M. A. Halim, M. A. Rub, M. A. Hoque, D. S. Islam, D. Kumar, Y. G. Alghamdi and A. M. Asiri, *J. Mol. Liq.*, 2020, **306**, 112880.
45 S. Ghosh and D. Rousseau, *Curr. Opin. Colloid Interface Sci.*, 2011, **16**, 421–431.